Towards Intelligent Synthetic Neural Circuits: Directing and Accelerating Neuron Cell Growth by Self-Rolled-Up Silicon Nitride Microtube Array

Supplemental Information

Paul Froeter,[1,¶] Yu Huang,[2,3,¶] Olivia V. Cangellaris,[4] Wen Huang,[1] Erik W. Dent,[5] Martha U. Gillette,[4,6] Justin C. Williams[2,*] and Xiuling Li[1,*]

[1] Department of Electrical and Computer Engineering, Micro and Nanotechnology Laboratory, University of Illinois at Urbana-Champaign, Urbana, IL 61801

[2] Department of Biomedical Engineering, University of Wisconsin-Madison, Madison, WI 53706

[3] Current address: Department of Nanomedicine and Biomedical Engineering, Houston Methodist Hospital Research Institute

[4] Department of Bioengineering, University of Illinois at Urbana-Champaign, Urbana, IL 61801

[5] Department of Neuroscience, University of Wisconsin-Madison, Madison, WI 53705

[6] Department of Cell and Developmental Biology, University of Illinois at Urbana-Champaign, Urbana, IL 61801

* xiuling@illinois.edu and jwilliams@engr.wisc.edu

¶ these authors contributed equally to this work

S1: Capacitance Vs Voltage (CV) analysis.

Fig. S1a shows a schematic of the fabricated metal-insulator-semiconductor (MIS) capacitor where the semiconductor substrate was n-type silicon with a resistivity was 3 Ω-cm (a doping density of $N_D \sim 2 \times 10^{15}$); the insulating layer was 200nm high frequency (HF) or 200nm low frequency (LF) silicon nitride thin film; and the metal layer was 200 nm thick evaporated aluminum (Al) thin film. All testing pads were 640 μm in diameter. As shown in Fig. S1b, we observed flat band voltage shifts for both bilayer components, LF and HF.

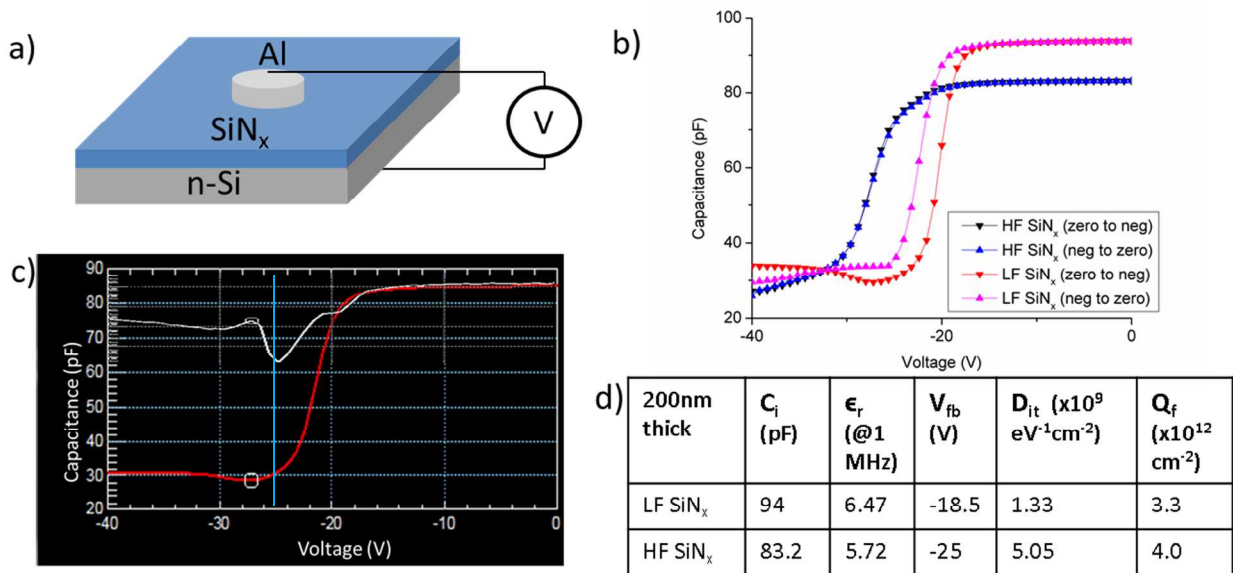| 200nm thick	C_i (pF)	ϵ_r (@1 MHz)	V_{fb} (V)	D_{it} ($\times 10^9$ eV^{-1}cm^{-2})	Q_f ($\times 10^{12}$ cm^{-2})
LF SiN$_x$	94	6.47	-18.5	1.33	3.3
HF SiN$_x$	83.2	5.72	-25	5.05	4.0

Figure S1 | Capacitance-Voltage (C-V) analysis of SiN$_x$ thin film. a) Metal insulator semiconductor (MIS) capacitor fabricated using 200nm thick high frequency (HF) or 200nm low frequency (LF) silicon nitride as the insulating layer on an n-Si wafer. In both cases 200nm of aluminum (Al) was deposited onto the insulating layer. b) High frequency (1 MHz) Capacitance-Voltage (HFCV) measurements of tensile HF- and compressive LF- SiN$_x$ reveal a large flat band voltage shift to the left, indicating a large quantity of fixed positive charges within the film. c) Quasi-static C-V (QSCV) measurement for 200nm LF SiN$_x$ film at 1kHz (white line) Vs high frequency measurement at 1MHz (red line). d) Summary of measured and extracted electrical parameters by HFCV and QSCV analysis reflecting a higher fixed charge and interface trap density for the HF SiN$_x$ film.

Note that a SiN_x film deposited under our high frequency recipe exhibits negligible hysteresis; a -25V shift is observed for either sweeping direction. However, SiN_x deposited under our low frequency recipe showed a -2 volt shift, from -18.5V when sweeping from zero to negative values (0V to -40V) to -20.5V when sweeping in the opposite direction. It is well known that fixed charges, as well as mobile charges, influence flatband shifts and hysteresis. Since these wafers were prepared and pre-cleaned using the industry standard RCA cleaning process, we can neglect mobile charges, simplifying our calculations. The 2V hysteresis observed here may be attributed to charging and discharging of K centers, altered by the previously applied bias[1]. There can also be a contribution to the flatband shift resulting from the formation of thin silicon or germanium oxynitride (SiO_xN_y or GeO_xN_y) films at the interface[2]. In order to combat this, both samples were cleaned in HF for the same amount of time, placed in methanol and dried with N_2 immediately before loading into the PECVD chamber. The fixed charge density can be extracted using Eq. 1-3[2].

$$Q_i = Q_f + Q_m + Q_{ot} + Q_{it} \tag{1}$$

$$C_i = \frac{(\epsilon_i * \epsilon_0 * A)}{d} \tag{2}$$

$$V_{fb} = \Delta\phi_{ms} - \frac{Q_i}{C_i} \tag{3}$$

Where Q_i is the insulator charge, Q_f is the fixed charge, Q_m is the mobile charge, Q_{ot} is the oxide trapped charge, and Q_{it} is interface trap charge densities. A is the area, d is thickness, and ϵ_o and ϵ_r are the free space and relative permittivity, V_{fb} is the flatband voltage, $\Delta\phi_{ms}$ is the metal-semiconductor work function difference (-0.213 V), and C_i is the insulator capacitance, which

we extracted from the high frequency capacitance vs voltage (HFCV) sweep at 1MHz. Further, we can extract the interface trap density D_{it} via a quasi-static (QSCV) comparison with HFCV, shown in Fig. S1c for a 200nm LF-SiN$_x$ film. In this case, HFCV was performed at 1 MHz and QSCV was performed at 1 kHz. Using Eq. 4 and extracted capacitances from QSCV v HFCV comparisons, we can accurately determine D_{it}.

$$D_{IT} = \frac{1}{q} * \left(\frac{C_i C_{lf}}{C_i - C_{lf}} - \frac{C_i C_{hf}}{C_i - C_{hf}} \right) \tag{4}$$

C_{lf} (the quasi-static capacitance) is measured at the minimum (64 pF for LF film shown by blue line) and C_{hf} is the high frequency capacitance and is measured at the same voltage (30 pF for LF film). Likewise, for the HF-SiN$_x$ film we extracted 61 pF for C_{lf} and 48 pF for C_{hf}. Assuming no mobile charges or oxide trapped charges, we can simplify Eq. 1 to only reflect fixed charges and interface trapped charges, those that are of concern to us, and successively solve for fixed charge density. We arrive at the relation:

$$Q_f = \frac{C_i}{Aq} * \left(\Delta \phi_{ms} - V_{fb} \right) - Q_{it} \tag{5}$$

The resulting charge densities, as well as relative permittivity (a useful quantity when determining the capacitance at a variety of bilayer thicknesses and ratio), are summarized in Fig. S1d for a 200nm SiN$_x$ film, thus we will need to normalize the fixed charge density to 20nm. The extracted Q_f would therefore be 4×10^{11} cm^{-2} in the 20 nm HF-SiN$_x$ and 3.3×10^{11} cm^{-2} in the 20 nm LF-SiN$_x$. When sweeping from negative voltages (rest at -40V for 5 sec, sweep -40V to 0V), LF films will charge to 3.7×10^{11} cm^{-2} corresponding to a flatband shift at -20.5V.

S2: FEM modeling of the electrostatic charge distribution for the tube array.

To visually grasp the electrostatic environment experienced by the neuron, we performed FEM modeling to generate the quasi-static electric field shown in Figure S2. Note that the simulation assumed the microtube array was supported by an electrostatically neutral substrate in air at room temperature. The operation frequency was set at 1 Hz, which has a corresponding wavelength (3×10^8 meter), much larger than the tube dimension; the charged tube structure was treated as a conductor, in which trapped charges was modeled as current flow; and lumped sources were used to feed different power levels into each microtube. The value of each feed in power was set up in simulation according to the positive charge density extracted from C-V analysis. The charge density in the microtubes was calculated by summing the contribution from the HF- and LF- SiNx sublayers within the film. Therefore, by assuming charges were uniformly distributed on the surface at a constant density, a quasi-quantitative field distribution can be achieved. The microtube opening was set to 1 Watt feed-in power and the center point of sidewalls to 0.7 Watt feed-in power, reflecting the respective geometry. Plotted electric field is normalized to 1 Watt input power of center tubes. Using time varying input power to simulate the static charge distribution would inevitably introduce inaccuracy of the calculation of E field intensity, so the relative value is given here instead of absolute value just to show the field distribution pattern which is reliable and fit the experiment very well.
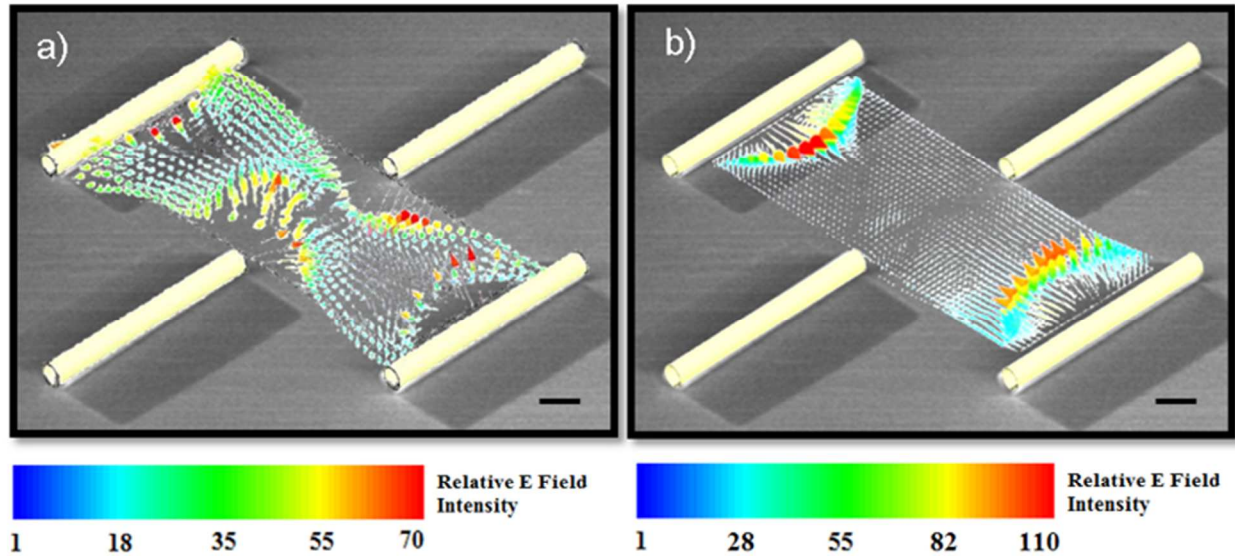
Figure S2 | Electrostatic Properties of SiN$_x$ microtube array. Superimposed SEM images of a microtube array (scale bar: 10 μm) with respective mapping of electric field lines between the microtubes with a longitudinal spacing of 40 μm. a) microtube arrays with charge density reflecting 20nm thick LF-SiN$_x$ on the outside of the microtube and 20nm HF- SiN$_x$ on the inside and b) microtube arrays with charge density reflecting 20nm thick LF-SiN$_x$ on the outside and 20nm HF- SiN$_x$ on the inside, however a layer, such as Al$_2$O$_3$, is added in the inside to mask the positive charge radiating from the microtube opening. (Simulation was done using High Frequency Structure Simulator version 11 software)

S3: Control cultures on coverslips with and without SiN$_x$ coating (~40 nm thick).

To test if the SiN$_x$ thin film itself has any effect on cell growth without the 3D geometrical confinement provided by the tube structure, we cultured neurons on control samples that are made of planar SiN$_x$ film coated glass coverslips and compared with bare glass coverslips under the same initial seeding density. Primary neurons were used for this comparison. As shown in the fluorescent stain (Fig. S3a, b) and summarized in the Table in c), the cell density at 4DIV is much higher (nearly doubled) on the planar SiN$_x$ bilayer coated coverslip, compared to that on the normal coverslip. This suggests that the SiN$_x$ substrate provides better cell adhesion and is

thus a more attractive substrate than glass for cell culturing. Since the initial seeding density was the same for the glass and SiN_x substrates, and the cultures were performed simultaneously, it is possible that the variability in final cell count at 4DIV is a factor of fewer cells attaching to the glass coverslips at the initial time of seeding; therefore, the perceived increase in cell adhesion on the SiN_x may just be a variable factor that will be corrected as the sample size increases. In order to truly determine whether survivability is similar between these two substrates, additional studies are underway.
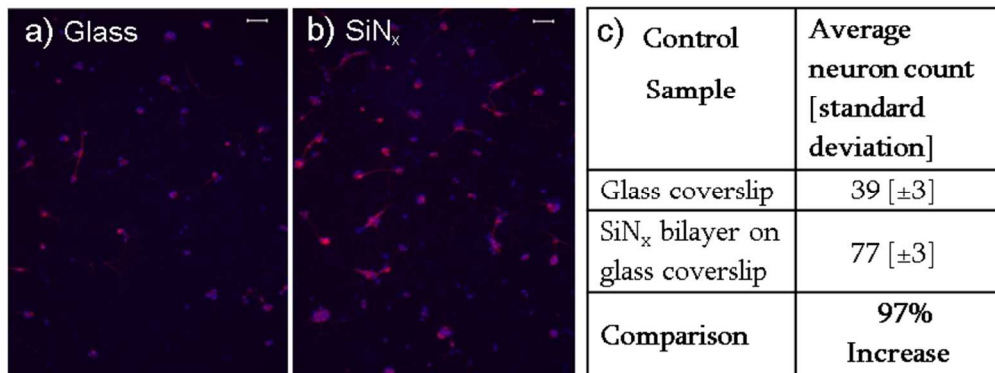

c) Control Sample	Average neuron count [standard deviation]
Glass coverslip	39 [±3]
SiN$_x$ bilayer on glass coverslip	77 [±3]
Comparison	97% Increase

Figure S3 | Comparison of neural culture on 2D planar control samples. MAP2 and DAPI staining of hippocampal neurons cultured on a) a PDL coated glass coverslip and b) a PDL coated 40nm SiN_x film deposited atop a glass coverslip (scale bar 50μm). c) Comparison (sample size n=3) of control sample characteristics: average number of neurons. An unpaired Student's t-test (one-tailed) was conducted for the cell number. The difference of average number of neurons between two groups are statistically significant (p-value < 0.05), indicating a substantial increase in cell adhesion to the SiN_x bilayer, compared to the glass coverslip.

Primary hippocampal neurons were harvested from postnatal day two (P2) Long-Evans BluGill rats (University of Illinois at Urbana-Champaign). The animals were used in accordance with the protocols established by the University of Illinois Institutional Animal Care and Use Committee, as well as all state and federal regulations. The hippocampi were isolated in Hibernate-A (Brain-Bits, Springfield, IL) and the dissociated neurons were cultured Neurobasal-A without phenol

red (Invitrogen) media. Each medium was supplemented with 0.25% GlutaMAX™ (Invitrogen), 2% B-27 (Invitrogen), and 1% 100 U mL^{-1} penicillin and 0.1 mg mL^{-1} streptomycin (Sigma-Aldrich). The primary culture protocol was adapted from Millet *et al.* [3]. The brain hippocampi were dissected and removed to ice-cold Hibernate-A. Four hippocampi from two rats were pooled in Hibernate-A with activated papain (25 U mL^{-1}, Worthington) and treated at 37°C for 15 min with agitation every 5 min to maintain separation of the tissue for complete exposure to the enzyme. The enzyme was aspirated and the tissue was washed with enzyme-free Hibernate-A. Fresh Hibernate-A was added and the cells were mechanically dissociated by trituration with a fire-polished glass Pasteur pipette. After the undissociated tissue settled, the supernatant was transferred to a new 15-mL conical tube, and the trituration was repeated with new Hibernate-A. Then, the enzyme treatment, wash, and mechanical dissociation were repeated. Next, the combined cell suspension was centrifuged at 1400 rpm for 5 min and the cells were re-suspended, counted, and diluted in Neurobasal-A. PDL-coated SiO$_2$ and SiNx-bilayer/SiO$_2$ coverslips were seeded at a density of 150-200 cells mm^{-2} for the 4 DIV cultures and 600 cells mm^{-2} for the 3 DIV culture. Cultures were kept in a humidified incubator at 37°C with 5% CO$_2$ until fixation at 3 or 4 DIV.

After 4 DIV, the cultures were fixed with 4% paraformaldehyde for 20 min, permeabilized with 0.3% Triton X-100 in PBS for 10 min, and blocked in 5% normal goat serum (NGS) in PBS for 30 min, all at room temperature. Between each step, the cultures were washed with PBS. Cultures were stained with rabbit poly-clonal anti-MAP2 (1:1000, Chemicon), and mouse mono-clonal anti-GFAP (1:1000, Chemicon) to label the dendrites and identify astrocytes, the cells, respectively. The primary antibodies were incubated for one hour at room temperature, then incubated at 4°C overnight. The following day, the cultures were washed with PBS, then

secondary antibodies were added and incubated for one hour at room temperature: Alexa Fluor 594 goat anti-rabbit (1:1000, Molecular Probes); Alexa Fluor 488 goat anti-mouse (1:1000, Molecular Probles). Finally, the cultures were stained with DAPI (1:50000, Invitrogen) for 10 min at room temperature to identify cell nuclei. Following a final PBS wash, the cells were stored in fresh PBS until imaging. Cultures were imaged on a Zeiss Axiovert 100 TV fluorescence microscope, as well as on a Nikon Optiphot-2 fluorescence and phase-contrast microscope.

S4: Culture on parallel strips of SiNx films on a Si substrate

The preferential attachment to SiN_x film observed above most likely is due to the electrostatic effect, since the SiN_x film is positively charged as indicated by the CV analysis (Fig. S1). However, since the mechanical stiffness of glass and SiN_x differ, glass coverslips have Young's Moduli of 72.9 GPa whereas SiN_x is approximately 170GPa, further experiments are needed. In Fig. S4, we compare axon outgrowth on silicon (111) and SiN_x thin film that have similar Young's Moduli (~170 GPa) but with vastly different surface charge properties. 10 nm thick of HF SiN_x was deposited on a silicon (111) substrate and patterned into 8.4 μm wide stripes separated by 6.6 μm. SEM of this culture (Fig. S4) shows superior attachment to the SiN_x strips, despite the similar Young's Modulus. The improved attachment to SiN_x is obvious from the cell

density on planar control samples (Fig S3c), but the guidance seen in Fig. S4c is exceptional, maintaining trajectory over 100 μm. Note that the process is guided down the center of this 10 nm thick membrane, rather than at the step edge or within the trench. In further support, both lines and trenches were uniformly coated with PDL and should have the same base charge density, thus enhanced attachment must be driven by electrostatic properties intrinsic to the SiN$_x$ film.
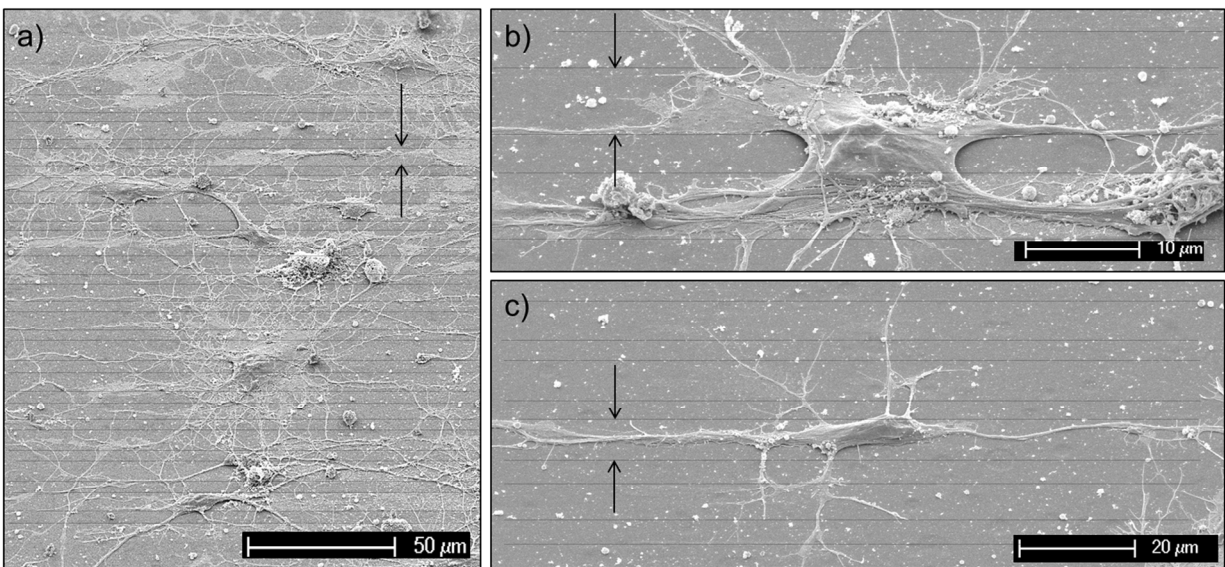

Figure S4 | SEM imaging of hippocampal cell culture on SiN$_x$ strips patterned on a Si(111) substrate. The SiNx parallel strips (indicated by the faint horizontal lines and arrows) are 10 nm thick, 8.4 μm wide separated by 6.6 μm. (a) showing preference for SiN$_x$. b) Extensions grow out and onto SiN$_x$ when the cell lands in between two strips and c) cells maintained linear guidance for over 100 μm on planar SiNx strips.

S5: 3D rendering of the confocal images and analysis

Figure S5 shows the 3D rendering of the confocal image of axonal growth of two neurons grown along the outer edge (A) and inside (B) binocular microtube structures, respectively. It turns out that the axons grown through the tubes demonstrated vastly different morphology as compared to that outside of tubes. They seem to take the shape of microtubes by filling the tube inner space for the most part with a height of ~ 2 μm. In contrast, axons that grow outside the microtube tend to flatten out show a height no more than 1 μm.
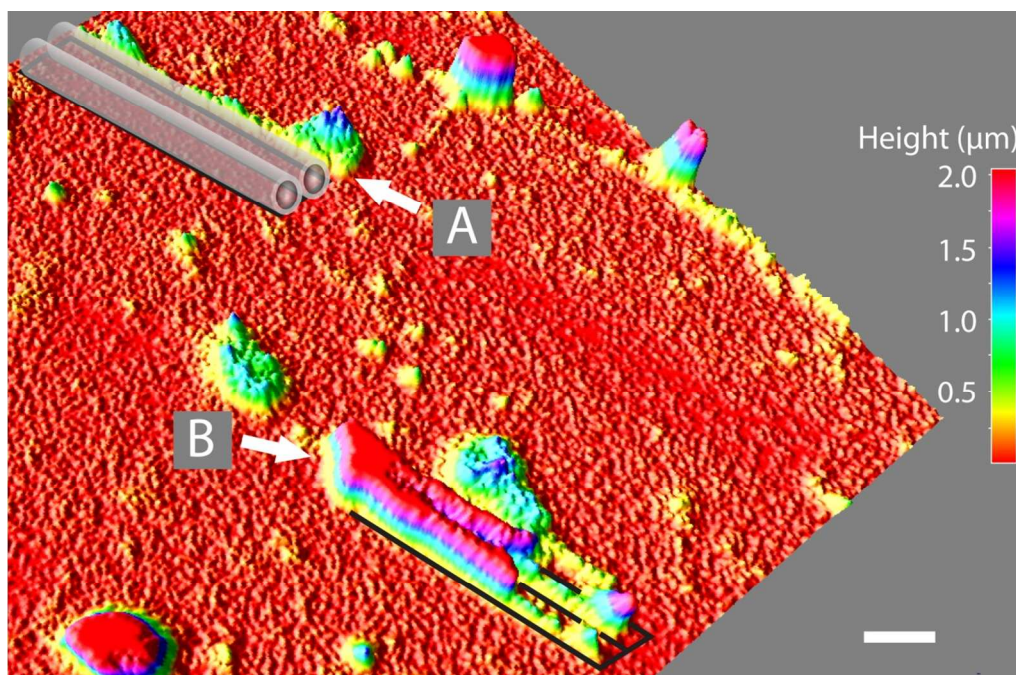

Figure S5 | 3D rendering of confocal image of axonal growth of two neurons (in white arrow). The cells were cultured in low density on binocular microtubes-contained substrate, in the same setting as that in Fig. 1c&d. A), an axon grows along the outer edge of a binocular structure, which is simulated in grey. Like neural culture on open substrate, this axon tend to flatten out with a height no more than 1 μm. B), two single axons grow inside each microtube of binocular structure. The tube position in projection is marked with black frames. Inside tube, these axons demonstrated vastly different morphology as compared to that out of tube. They seem to take the shape of microtubes by filling the tube inner space. For the most part, axon's height became 2 μm. (Scale bar: 5μm)

S6: Immunocytochemistry fluorescence images

Based on all the Immunocytochemistry fluorescent images examined (Figure S6), there is a strong tendency to continuously follow the linear array of microtube pattern, with very few off-pattern growth (indicated in white arrows). The fraction of axons that follows pattern is estimated to be ~83%.
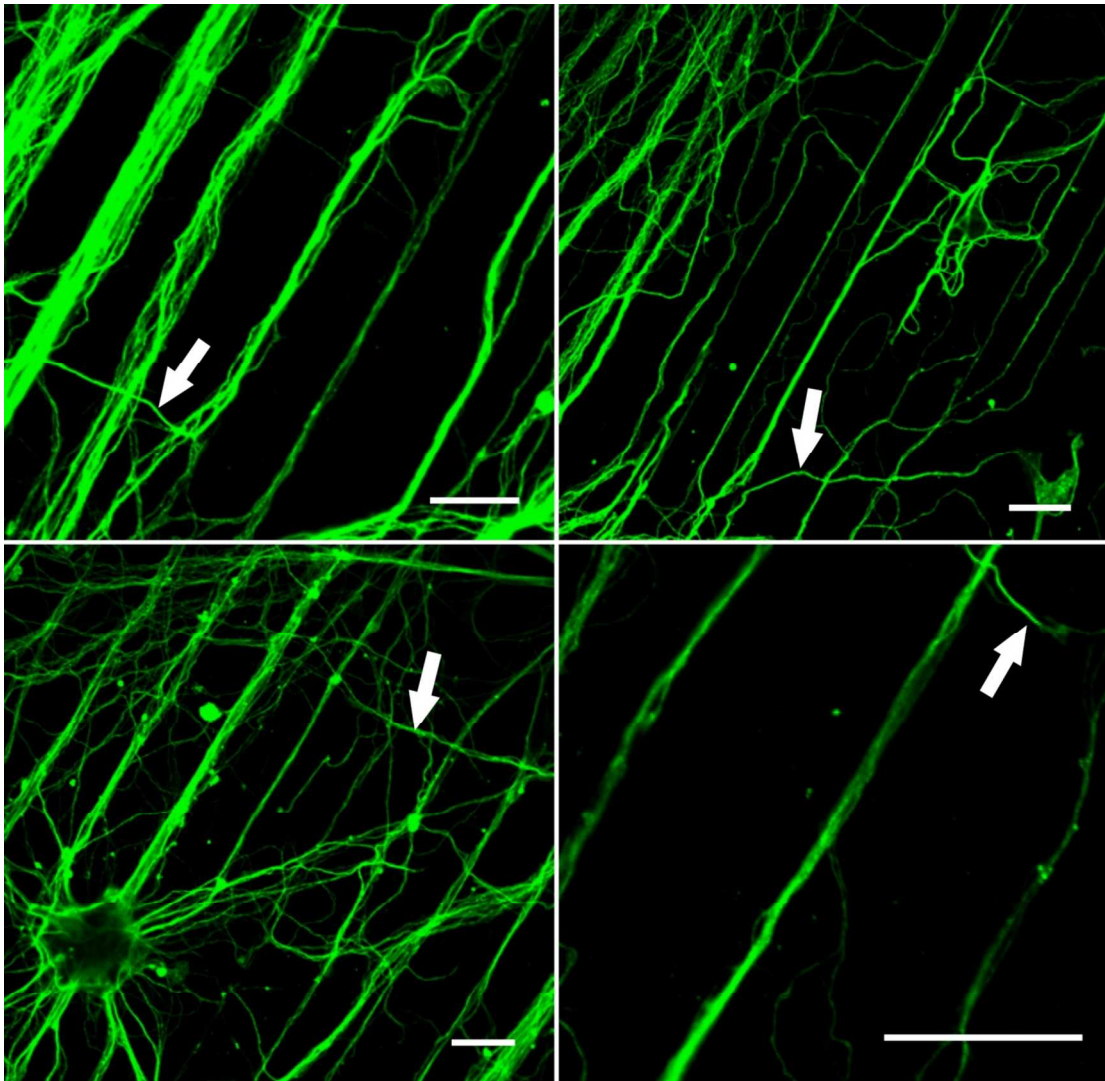

Figure S6 | Immunocytochemistry of neural culture on single-roll microtube arrays. The microtube patterns used here were identical to that shown in Fig. 1a. All fluorescent images indicated a strong tendency to continuously follow these patterns in a linear trajectory, with very few off-pattern growth (in white arrows). The fraction of axon that follows pattern is ~83%. (Scale bar: 50 μm.)

S7: Live cell recording of neuron outgrowth in microtubes.

Uniquely flexible fabrication of microtube arrays allow for the use of optically transparent glass coverslip as the supporting substrate. We conducted phase contrast live-cell imaging to capture long-term cell growth dynamics and axonal pathfinding in microtubes. Herein, two scenarios are exemplified in video S1. Video S1.a) presents a scenario in which the axonal growth cone follows the microtube array in a linear fashion, successfully growing through the tube opening. The growth cone was guided by the tube until exiting at the other end, returning to the 2D planar substrate. Video S1 b) presents a scenario in which through-tube guidance was chosen after the neuron surveyed the surrounding microtubes. A growth cone first reached outer wall of the microtube (instead of microtube opening), slowly guided by the half-confined outer corner of tube. Once the neuron sent out another process that reached near tube opening, the previous process was retracted, extending a new branch to grow through microtube. In both scenarios, the growth cone displayed an increased outgrowth velocity inside the microtube as compared to outside of the tube region on the 2D planar substrate, especially immediately upon entry. The detailed analysis of outgrowth velocity and representative frames are illustrated in Fig. 2(b, c).

a)

b)
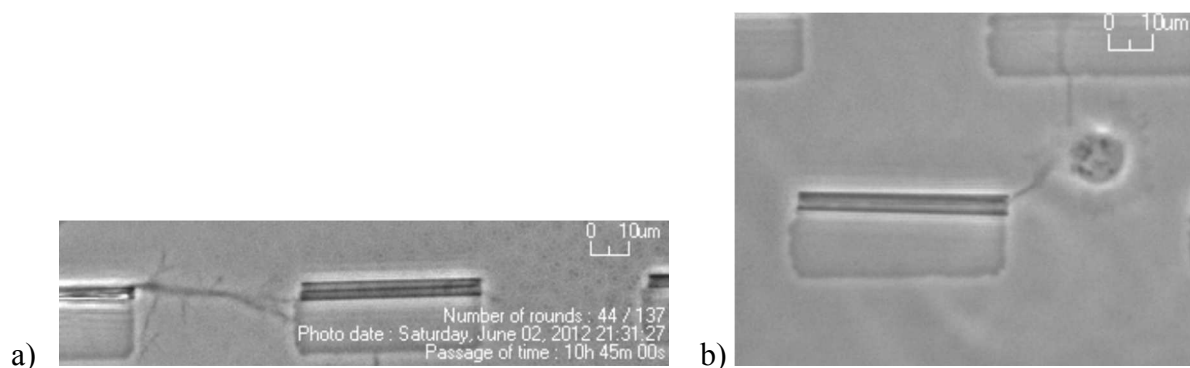
Video S1 | Live cell recording of neuron outgrowth on a substrate with a SiN$_x$ microtube array. a) A growing axon was guided by an array of microtubes in a linear fashion (from left to right). The entire pathfinding of the growth cone that enters, grows through, and exits a microtube was captured over the

course of ~1.5 days with 15-minute increment. b) Pathfinding of an axon that started by surveying the surrounding of the microtubes, branching one process while retracting another, before reaching a tube opening and growing through the microtube (from right to left).

References

1.   Beylier, G., et al., New Characterization Methodology of Borderless Silicon Nitride Charge Kinetics Using C-V Hysteresis Loops. Journal of The Electrochemical Society, 2008. 155(5), pp. H273-H279. *Journal of The Electrochemical Society* **2008,** *155* (5), H273-H279.
2.   Aberle, A. G. Crystalline silicon solar cells: advanced surface passivation and analysis. Sydney: University of New South Wales, 1999.
3.   Millet, L. J.; Stewart, M. E.; Sweedler, J. V.; Nuzzo, R. G.; Gillette, M. U., Microfluidic devices for culturing primary mammalian neurons at low densities. *Lab Chip* **2007,** *7* (8), 987-94.